J. Fluid Mech. (1986), *vol.* 169, *pp.* 125–149
Printed in Great Britain

Unstable jet–edge interaction. Part 1. Instantaneous pressure fields at a single frequency

By RUHI KAYKAYOGLU AND DONALD ROCKWELL
Department of Mechanical Engineering and Mechanics, Lehigh University, Bethlehem, PA 18015, USA

(Received 22 August 1984 and in revised form 17 September 1985)

Despite its central importance, the pressure field at a leading edge has remained uncharacterized for the classical jet–edge interaction at a single predominant frequency. This investigation shows that the force, due to the integrated instantaneous pressure field on the edge, is located a distance downstream of the tip of the edge as much as one-quarter of a wavelength (λ) of the incident instability; this distance also corresponds to about one-quarter of the geometric length (L) between the nozzle and tip of the edge. Consequently, the traditional assumption that the phase-locking criterion for self-sustained oscillations can be expressed as a ratio of L/λ is inappropriate for low-speed jet flows, which have been of primary interest over the past two decades.

The edge pressure field is made up of two regions bounded by the maximum amplitude at the onset of separation from the surface of the edge: a near-tip region ($0 \leqslant x/\lambda \lesssim 0.1$) where the amplitude drops to a minimum as the tip is approached; and a downstream region ($x/\lambda \gtrsim 0.1$) where the amplitude varies as x^{-a}. Since the drop in pressure in the near-tip region does not occur over a streamwise length commensurate with the length of the edge, imposition of a Kutta condition is inappropriate in simulations of the edge region. Moreover, in the near-tip region ($0 \lesssim x/\lambda \lesssim 0.2$), the pressure field is non-propagating; a wave-type representation is appropriate only downstream of this region.

At the tip of the edge, occurrence of the pressure minimum is due to the minimum in fluctuating angle of attack α of the approaching shear layer, deducible from the velocity eigenfunctions of linear theory; correspondingly, flow separation occurs downstream of, not at, the tip of the edge. When the tip is displaced off centreline, there is a rise in α, giving a rise in tip pressure amplitude; nevertheless, the overall x^{-a} amplitude distribution persists.

This overall x^{-a} ($a \sim \frac{1}{2}$) variation of the pressure amplitude commences downstream of the tip of the edge near the onset of flow separation, which leads to secondary-vortex formation; in turn, it is driven by development of the primary vortex in the unstable jet shear layer, having initially distributed vorticity. The role of this flow separation and subsequent secondary-vortex formation is, therefore, not to relieve a singularity at the tip of the edge; it is simply a consequence of growth of the primary vortex along the edge.

1. Introduction

The interaction of an unstable shear layer with a leading edge occurs in a range of hydro/aeroelastic and acoustic applications; it is crucial in determining the fluctuating pressure field on the surface of the edge and thereby noise radiated from

the leading portion of the body. Moreover, such interactions set the stage for the transition process to a turbulent boundary layer immediately downstream of the leading-edge region.

Theoretical simulations of leading-edge interactions include cases of either planar acoustic waves or vortical disturbances incident upon a leading edge. For the situation of an acoustic wave interacting with the edge, both Goldstein (1981) and Howe (1981) include consideration of the downstream-travelling instability waves along the surface of the edge, as well as the nature of the diffracted field. In both of these studies, the authors address the amplitude of the induced fluctuation level in the leading-edge region, but take independent approaches, as discussed in the reviews of Crighton (1981) and Rockwell (1983). A central difference is the role played by the instability of the approach shear layer relative to that of the boundary layer on the surface of the edge. Howe takes the viscous layers on the edge surface as supporting amplifying instability waves; their amplitude is determined by elimination of the pressure and velocity singularities at the tip of the edge. On the other hand, Goldstein asserts that the boundary layer on the surface of the edge cannot eliminate the singularities of pressure and velocity at the tip; instead, the inherently unstable approach flow remains unstable as it negotiates the edge. Its instability evolves in a fashion independent of the scales of the viscous layer on the surface of the edge.

Another formulation of the leading-edge problem replaces the incident acoustic wave with a propagating vortical disturbance. As in the foregoing, this inviscid analysis also includes the nature of the mean vorticity approaching the edge. Goldstein (1978, 1979) analyses this class of problems by employing the concept of rapid distortion in the leading-edge region. One is left, however, with the dilemma of whether a leading-edge Kutta condition or causality is more appropriate.

It is clear that much has been advanced in conceptually relating the growth of instabilities downstream of the edge to disturbances incident upon it. To allow tractable analysis, however, the theoretical approaches invoked to date have not embodied the complex physical details of the leading-edge region which, under certain circumstances, may involve significant nonlinear and viscous effects. In fact, there has been no experimental clarification of the leading-edge region for the fundamental, and much investigated, case of a self-excited planar jet incident upon an edge (Powell 1961; Rockwell 1983). Even in the simplest case, where the vorticity field incident upon the edge region is distributed rather than concentrated in a vortex (Kaykayoglu & Rockwell 1985), physical interpretation of the edge interaction is complicated by strong gradients of the fluctuating velocities and their respective phases across the incident shear layer; correspondingly, the approach shear layer will have an angle of attack that varies substantially in the cross-stream direction. Consequently, one expects the nature of the instabilities along the upper and lower surfaces of the leading edge to be a strong function of the location of the edge within the incident shear layer.

In this investigation, we address the physical features of the flow in the near region of the edge and relate them to the instantaneous pressure fields on the edge surface. In particular, the heretofore uninvestigated features of primary interest are: the nature of primary- and secondary-vortex formation and interaction in the leading-edge region; and the consequent phase and amplitude variations of the fluctuating pressure fields in the leading-edge region.

2. Experimental system and instrumentation

Experiments were conducted in a recirculating water-channel system with a planar nozzle insert in its test section. The length of the parallel section of the nozzle relative to its width was 68, thereby providing a fully developed flow at the nozzle exit for the Reynolds number considered herein, $Re = 600$. This Reynolds number represents the best compromise between effective flow visualization, reasonable averaging times for the LDA and pressure-field measurements, and avoiding complexities of higher-order modes of the unstable jet. Moreover, in order to provide an essentially two-dimensional planar jet, the breadth-to-width ratio of the nozzle was 48. The ratio of the test-section height to nozzle width was maintained at 72, thereby minimizing possible influence of the lower bounding wall and the upper bounding free surface of the test section. By varying the dimensionless lengthscale L/w between the nozzle exit and impingement edge, it is possible to provide unstable jets of varying maturity, i.e. amplitude of oscillation, impinging upon the leading-edge; this allows examination of the effect of velocity-fluctuation amplitude immediately upstream of the edge on the flow patterns downstream of the tip of the edge. Herein, we employ two values of this lengthscale L/w: 3.25 and 4.50. At smaller values of L/w the oscillations became intermittent and at higher values the frequency content of the jet becomes more complex owing to onset of modulation and nonlinear interaction effects (Lucas & Rockwell 1984).

Velocity measurements of the approach flow were carried out with an argon-ion laser operated in the backscatter mode. Use of a beam expander allowed maximization of the signal-to-noise ratio from an optical standpoint; moreover, water was seeded with silicon carbide particles to provide uniform scattering. The Doppler signal was of sufficient quality that the analog output of the frequency counter could be employed. Both streamwise $\tilde{u}$ and transverse $\tilde{v}$ fluctuation components, as well as their respective phases $\phi_{\tilde{u}}$ and $\phi_{\tilde{v}}$ were determined. Herein, $\tilde{u}$ and $\tilde{v}$ denote time-averaged amplitudes determined from spectral analysis, and u' and v' the instantaneous fluctuation amplitudes of u and v. Spectral analysis of the signals followed from digital processing on a MINC minicomputer (LSI 11-23) with direct memory access. The phases of the velocity fluctuations were determined by cross-spectral analysis between the velocity (LDA) signal and a reference pressure signal on the surface of the edge. In carrying out spectral and cross-spectral analyses of the fluctuating velocity and pressure signals, 50 oscillation cycles were examined; furthermore, a total of six spectra were averaged to obtain the final amplitudes of the spectral components.

In order to measure the unsteady pressure field in the leading-edge region, we employed high-sensitivity Kulite pressure transducers with a paralene coating (XCS-190-2D). A total of nine pressure taps were located in the leading-edge region, one at the tip itself and the others on the upstream and downstream surfaces of the edge at distances from the leading edge of $x' = 0.16, 0.48, 0.96$, and 1.90 cm. In terms of the wavelength λ of the single-frequency instability wave along the surface of the edge, these distances correspond to $x'/\lambda = 0.067$, 0.2, 0.4, and 0.8, for the case $L/w = 3.25$; at a higher-value L/w, the wavelength λ was 20% larger, making the respective ratios x'/λ 20% lower. The tip of the edge was 0.05 cm thick, an order of magnitude smaller than the vorticity thickness of the incident jet defined as $U_{\text{¢}}/(\mathrm{d}\bar{u}/\mathrm{d}y)_{\max}$. Due to the small thickness of the tip and the small angle (30°) of the wedge shown in figure 1, it was necessary to stagger the pressure taps in the transverse z-direction. Successive taps were at distances of $z = 2.8, 4.1, 5.4$, and 6.7 cm from the

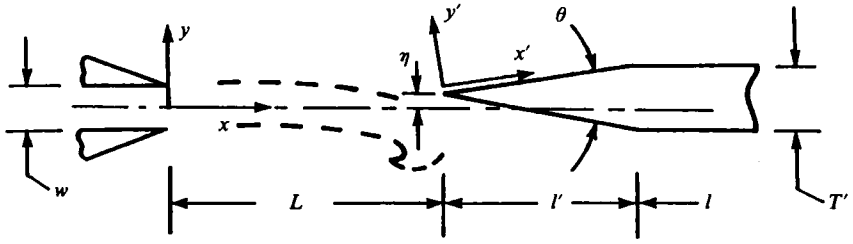

FIGURE 1. Overview of jet–edge system.

centreline of the edge. By extensive flow visualization, it was possible to demonstrate that the flow was two-dimensional in the spanwise direction over the domain of measurement. Moreover, to further ensure the essentially two-dimensional character of the oscillation, preliminary measurements were made at smaller values of nozzle breadth to width, with the impingement length L scaled accordingly; in essence, the same patterns of jet oscillation and interaction persisted.

The diameters of the pressure taps were 0.8 mm, except for the leading-edge tap, which had a diameter of 0.4 mm. The channels that connected these taps to the transducers had diameters ranging from 0.4 mm to 3.1 mm and lengths from 7.7 cm to 11 cm. Of prime concern in this type of arrangement is the possibility of amplitude and phase distortion due to the finite length (and volume) of the pressure tap, connecting channel and reservoir between the channel and the transducer face. At the characteristic frequencies of oscillation, maximum amplitude and phase distortion were 0.1 % and 0.2°, as determined by extensive frequency-response tests.

During experiments, two transducers were employed; one measured the fluctuations at the pressure tap of interest and the other served as a reference signal. Small valves located in each pressure line downstream of the edge allowed correlation of signals between the reference pressure tap and the selected active tap. Signal analysis involved a cross-spectral technique with a MINC minicomputer, which gave the amplitude and relative phase of the pressure at each tap under consideration. Then, taking advantage of the fact that the flow was essentially periodic, the instantaneous pressure fields were reconstructed in conjunction with the visualized flow patterns.

Flow visualization was accomplished using the hydrogen-bubble technique; bubbles were generated from a vertical platinum wire located at the tip of the edge; however, in most experiments, a dye-injection technique showing streaklines emanating from the upstream lips of the nozzle provided substantial details of the interaction mechanisms at the leading edge. By using an Instar IV television system having a split-screen capability it was possible to simultaneously record the instantaneous pressure fluctuations at a desired location on the surface of the edge with the visualized flow patterns. The Instar television system has horizontal and vertical frequencies of 25.2 kHz and 120 Hz, and a framing rate of 120 frames s^{-1} and a resolution of 250 lines.

3. Approach flow characteristics

Central to determining the nature of the instantaneous pressure field on the leading edge is the type of approach flow. Considerable effort was expended to generate a periodic shear layer incident upon the edge having the smallest possible, self-sustaining, fluctuation amplitude. In doing so, we precluded formation of vorticity

concentrations in the incident shear layer. In the flow region very near the edge, however, the interaction process itself produced rapid vortex formation.

To characterize the unsteady shear layer approaching the edge, we selected a location w upstream of the tip of the edge. Two different amplitudes of the approach-flow oscillation were generated by selecting two values of streamwise lengthscale L, $L/w = 3.25, 4.50$ (see §2); the longer one allowed the instability wave to reach a higher amplitude before negotiating the edge. Hereafter, these cases of small and large L/w are referred to as small- and large-amplitude oscillations respectively. Measurements were made of the fluctuation-velocity profiles of the streamwise $\tilde{u}(y)$ and transverse $\tilde{v}(y)$ fluctuating components and their respective phases $\phi_{\tilde{u}}(y)$ and $\phi_{\tilde{v}}(y)$, as well as the mean velocity distribution, well approximated by $\tilde{u}/U_{\mathbb{C}} = \mathrm{sech}^2 y$; these data and their approximation by linear stability theory are described in detail by Kaykayoglu (1984). The high-amplitude case ($L/w = 4.50$), relative to the low-amplitude case ($L/w = 3.25$), produced a substantially higher-amplitude distribution of $\tilde{u}$ (e.g. peak amplitude $\tilde{u}_{\max}$ of 0.095 compared with 0.070).

Using the foregoing amplitude and phase information, it is possible to construct the instantaneous velocity variations, as well as the angle of attack, of the incident flow at this reference station. At the jet centreline, the amplitude $\tilde{u}$ approaches zero, while the $\tilde{v}$-component can take on values as high as $0.04 U_{\mathbb{C}}$. Off centreline, both $\tilde{u}$ and $\tilde{v}$ can take on substantial values. If we now combine these fluctuating-velocity distributions with the corresponding mean distributions of u and v, it is possible to construct the instantaneous velocity vectors across the flow at successive instants of time. Figure 2 (*a*) shows the instantaneous angles of attack $\alpha(t)$ corresponding to these velocity vectors, where

$$\alpha(t) = \tan^{-1}\left[\frac{v'(y,t)}{[(u(y)+u'(y,t)]}\right].$$

Figure 2 (*b*) provides a summary of the time-averaged jet structure at this reference station including the amplitude of the angle of attack α_0, where $\alpha(t) = \alpha_0 \sin(\omega t + \phi)$. Also given is the kinetic-energy distribution across the jet $(\tilde{u}^2+\tilde{v}^2)/(\tilde{u}^2+\tilde{v}^2)_{\max}$ as well as the dimensionless velocity correlation $\overline{u'v'}/\overline{(u'v')}_{\max}$. It is evident that the higher-amplitude case corresponds to higher α_0 and $\tilde{u}^2+\tilde{v}^2$; consequently, the nature of the interaction at the edge should reflect this difference in approach-flow conditions.

The distributions of $\alpha(t)$ vs. y/b in figure 2 (*a*) and $|\alpha|$, $\tilde{u}^2+\tilde{v}^2$, and $\overline{u'v'}$ in figure 2 (*b*) are important in two respects. First, the remarkably small values of α and $\tilde{u}^2+\tilde{v}^2$ at the centreline of the jet suggest that there will not be flow separation at the tip itself; however, the relatively large values of fluctuating angle of attack in regions away from the centreline will, as the jet negotiates the tip region of the edge, give rise to large pressure gradients at the surface of the edge that may induce flow separation shortly downstream of the tip. Of course, this process is intertwined with the fluctuating vorticity and concentration of vorticity at the tip as given at the bottom of figure 2 (*a*). Moreover, one expects that if the edge were to be moved to a region away from the centreline of the oscillating jet, the flow structure in the leading-edge region would change substantially because of the larger fluctuating angles of attack away from the centreline, as well as changes in amplitudes of $\tilde{u}^2+\tilde{v}^2$ and $\overline{u'v'}$. We note the large transverse gradients of the latter two parameters at the centreline, suggesting high sensitivity of the leading-edge dynamics to small displacements of the edge.

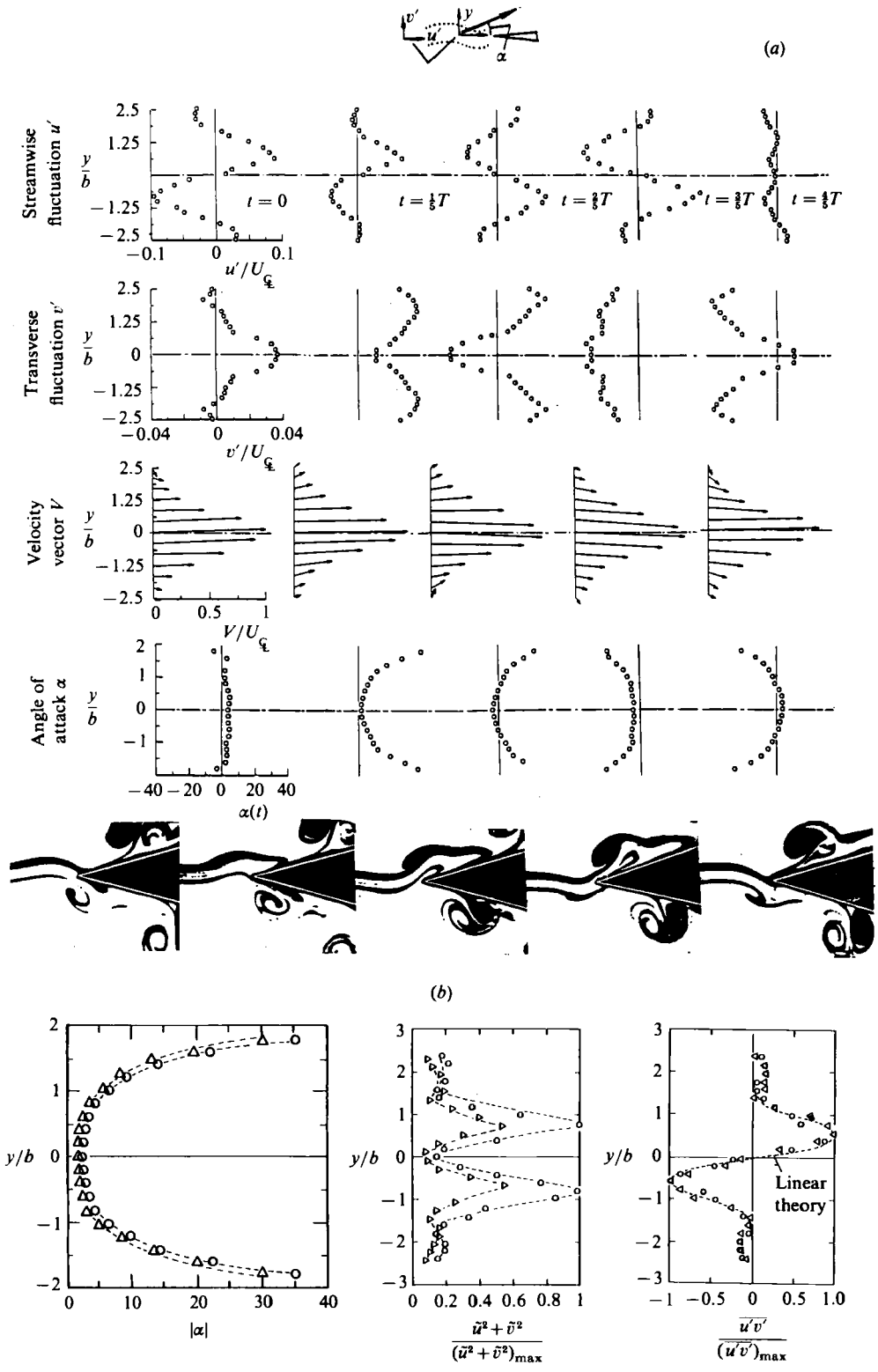

FIGURE 2. For caption see facing page.

4. Overview of flow in the leading-edge region

From the foregoing characterization of the unsteady shear layer incident upon the leading edge it is evident that the to-and-fro motion of the jet across the edge will give rise to unsteady wavelike motions along the upper and lower surfaces of the edge. Figure 3 (*a*) shows these time-dependent flow patterns for the low and high oscillation amplitudes of the incident jet described in the foregoing. The left column of figure 3 (*a*) depicts the lower amplitude, and the right column the higher amplitude. In both cases, the transverse oscillation of the jet promotes rapid formation of a primary vortex as the tip of the edge is negotiated; the sense of rotation of this vortex is compatible with that of vortex formation in the corresponding non-impinging jet. A secondary vortex arises immediately downstream of the tip region, thereby forming a vortex pair with the primary vortex. These vortex pairs then move downstream together. An apparent difference between these low- and high-amplitude cases of figure 3 (*a*) is that the scales of the primary and secondary vortices are larger for the former; moreover, the counter-rotating vortex pairs of the higher-amplitude case tend to move away from the surface of the edge at relatively small distances from the tip, whereas the counter-rotating vortex pairs of the lower-amplitude case tend to move along the surface of the edge.

Figure 3 (*b*) compares the visualized vortex patterns along the surface of the edge for several types of flow visualization: dye emanating from the upstream nozzle lips (left column); a sheet of hydrogen bubbles liberated from a wire located at the tip of the leading edge (middle column); and dye injected through a small pressure tap at the tip of the leading edge (right column). For all types of visualization, the nature of the primary- and secondary-vortex formation is very similar. In the right column of photos, the movement of the dye streakline away from the wall during formation of the secondary vortex occurs quite near the tip, suggesting that there are large velocity and pressure gradients in that region.

Figure 4 shows visualization with dye-injection and hydrogen-bubble techniques. The bubble wire is located at the tip of the leading edge, and the timelines are generated at constant frequency. Consequently, when the local flow dynamics produces timelines further apart, or closer together, there is a direct indication of, respectively, local acceleration or deceleration. By observing a single cycle of oscillation over ten instants of time, i.e. at photo intervals of 0.1 T, where T is the period of oscillation, we attempt to describe in further detail the primary- and secondary-vortex formation of figure 3. In doing so, it is helpful to classify the local flow dynamics into the three phases indicated in figure 4: (I) onset of primary-vortex formation; (II) development of primary vortex and onset of flow separation; and (III) development of secondary vortex.

In phase I, depicted in figures 4 (*a–c*), one sees that downward deflection of the jet produces flow acceleration in the tip region (figure 4*a*). In the region away from the tip of the edge, shown in the lower parts of figures 4 (*a–c*), there is onset of reverse flow, corresponding to formation of the primary vortex. (Compare with adjacent dye-visualization photo.) In fact, one already sees in figure 4 (*b*) formation of a distinct

---

FIGURE 2. (*a*) Distributions of instantaneous values of streamwise $\tilde{u}$ and transverse $\tilde{v}$ velocity fluctuations, instantaneous velocity V, and instantaneous angle of attack α as a function of transverse location in the incident shear layer. (*b*) Distributions of amplitude of angle of attack α_0, dimensionless kinetic-energy amplitude $[\tilde{u}^2+\tilde{v}^2]/[\tilde{u}^2+\tilde{v}^2]_{\max}$, and dimensionless velocity correlation $\overline{u'v'}/(\overline{u'v'})_{\max}$ across the incident shear layer: ○, $L/w = 4.5$; △, 3.25.

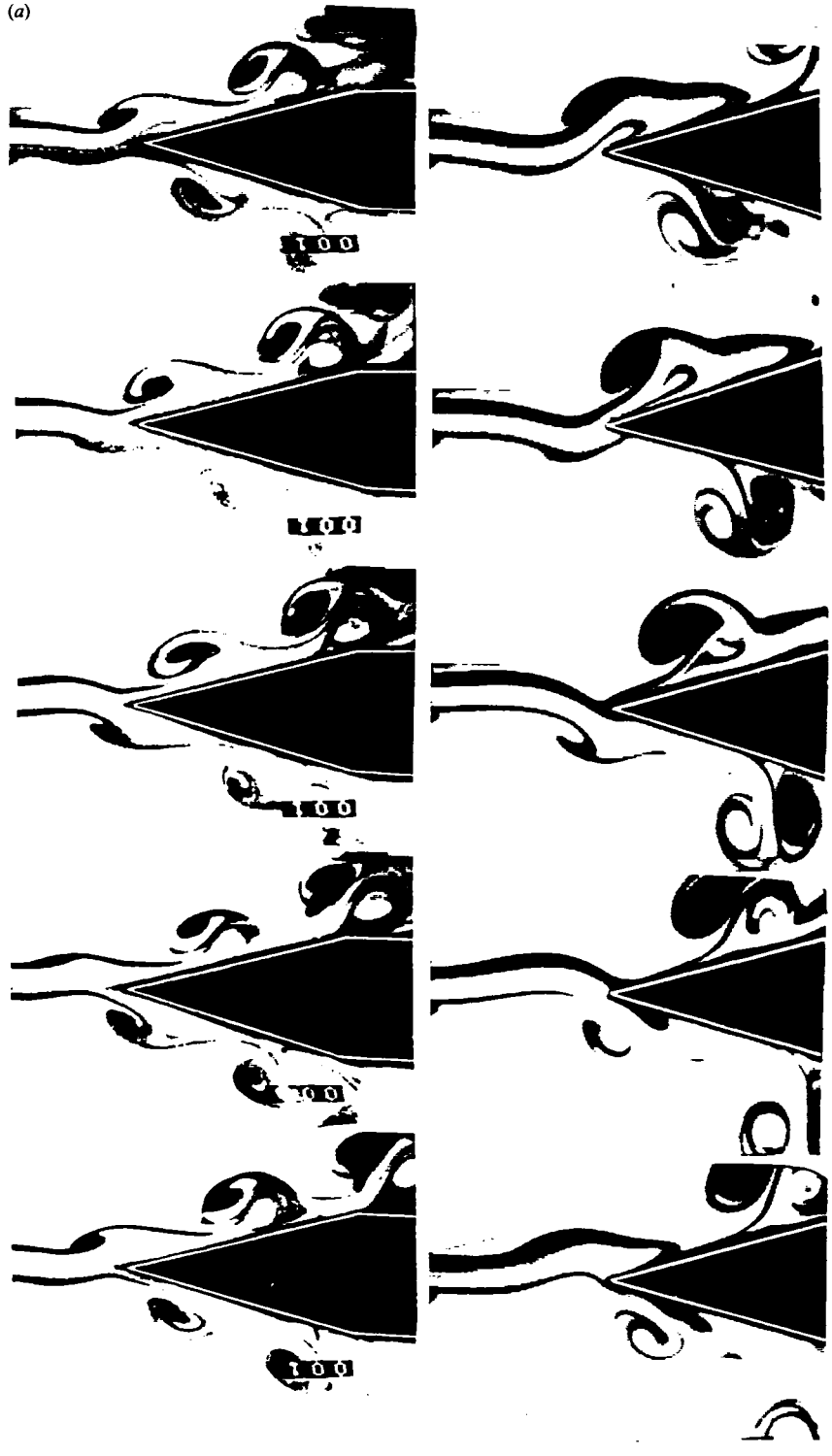

FIGURE 3. For caption see facing page.

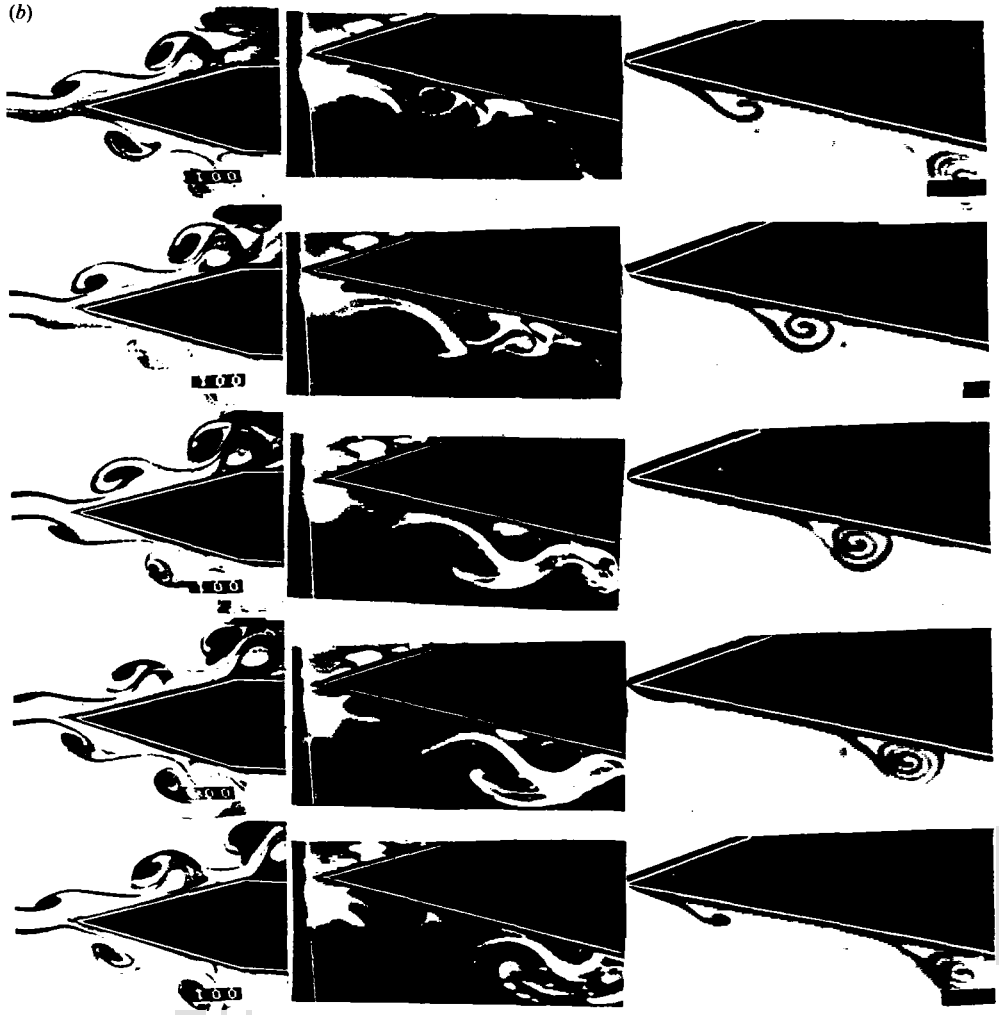

FIGURE 3. (*a*) Comparison of jet–edge interaction pattern for relatively low- ($Re = 600$; $L/w = 3.25$) and high- ($Re = 600$; $L/w = 4.5$) amplitude fluctuations of the incident jet. (*b*) Visualized patterns of vortex formation at the leading edge for lower-amplitude jet by dye streaklines emanating from the upstream lips of the nozzle, hydrogen bubbles released from wire located at the leading edge, and dye injected through the leading-edge pressure tap.

surface O–A between the forward flow near the tip of the edge and the onset of reverse flow in the region well below the tip, i.e. below point O. In the next sequence of photos, we follow point O as it is swept downstream of the bubble wire, staying with the centre of the primary vortex.

In phase II (figures 4*d–f*), there is onset of flow separation from the surface of the tip, evident in figure 4(*e*) and more pronounced in figure 4(*f*). This flow separation is associated with development of the primary vortex and formation of a surface whose leading edge is designated as B; this surface represents the boundary between high-speed fluid of the primary vortex and low-speed fluid which eventually is swept in the opposite direction to form the secondary vortex.

In phase III, initiating with figure 4(*g*), the onset of secondary-vortex formation

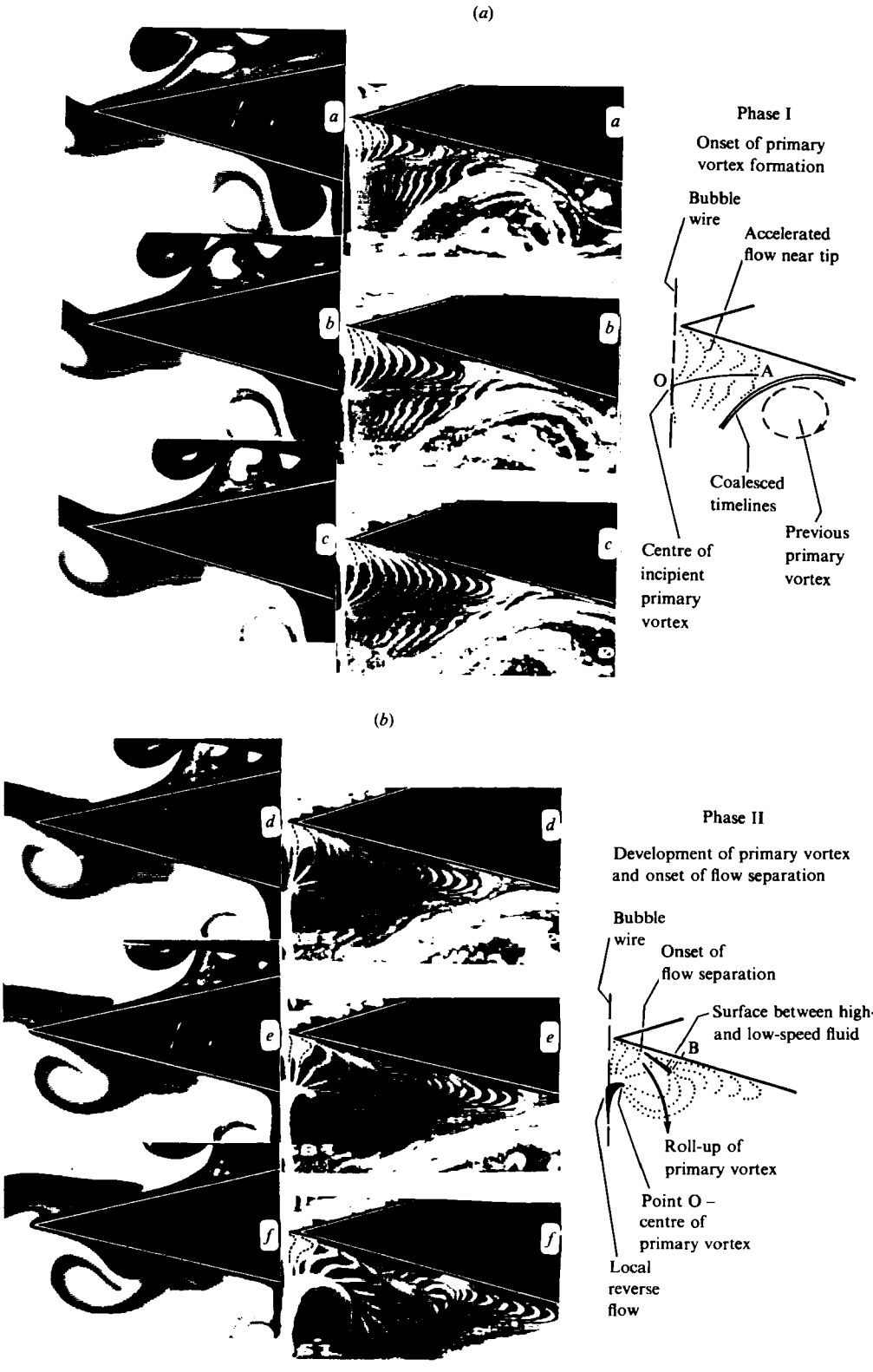

FIGURE 4(*a*, *b*). For caption see facing page.

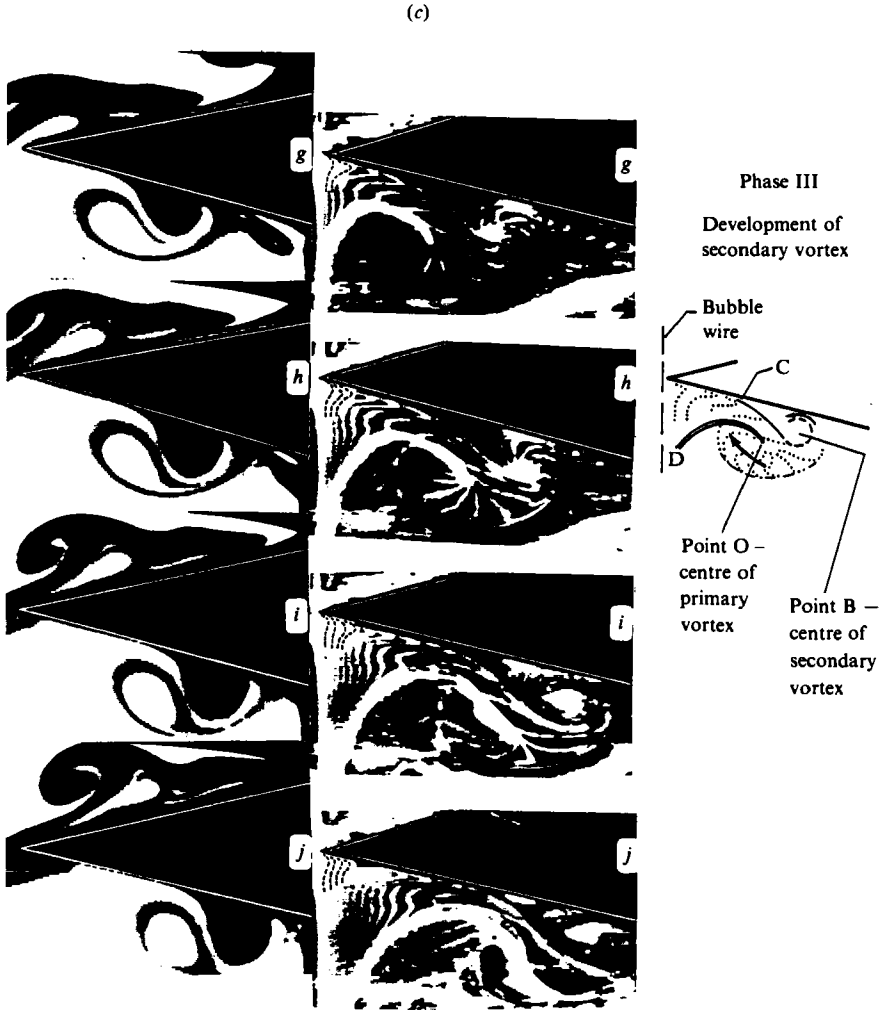

FIGURE 4. Three basic phases of primary- and secondary-vortex formation in the leading-edge region showing: accelerated flow in vicinity of tip; onset of flow separation immediately downstream of tip; and roll-up of primary and secondary vortices ($L/w = 4.5$). (*a*) Phase I; (*b*) Phase II; (*c*) Phase III.

is clearly detectable as the primary vortex continues to roll-up. This process continues in figures 4(*h–j*). In the sketch adjacent to figure 4(*h*), we indicate the two surfaces associated with the primary–secondary vortex-pair combination; surface B–C, which together with the wall surface bounds the fluid that is ingested into the secondary vortex; and surface O–D which represents the analogous surface of the primary vortex, i.e. fluid below it, from the external stream, is ingested into the primary vortex. Point O corresponds to the leading tip of bubble lines that earlier coalesced at the bubble-wire location due to reverse flow there (figure 4*f*); it has become the apparent centre of the primary vortex in figure 4(*h*). The area between these two surfaces O–D and B–C contracts such that they nearly touch; correspondingly, the flow between them substantially accelerates. At even larger values of time, as indicated in figure 4(*c*), it appears that there is no flow between the two surfaces,

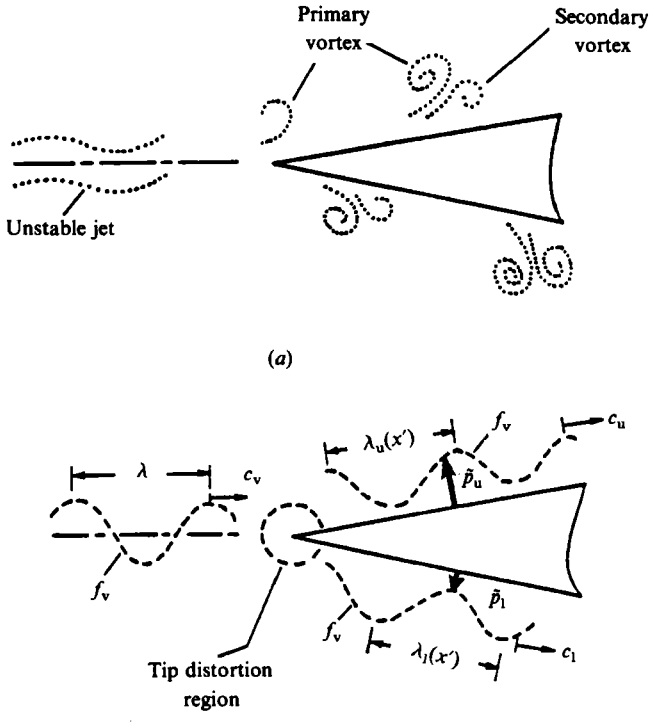

FIGURE 5. Schematics of (*a*) unstable jet interacting with leading edge, and generation of primary and secondary vortices; and (*b*) wavelike representation of incident jet shear layer and pressure fields along upper and lower surfaces of the edge.

meaning that the vortex-pair combination has grown by entraining fluid from the regions surrounding the primary and secondary vortices. While the foregoing phenomena occur, it is evident that the distance between the separation point and the centre of the secondary vortex continues to increase (see figures 4*g–j*).

From this flow visualization, one expects large pressure fluctuations in the region near the tip where there is onset of flow separation, leading to formation of the secondary vortex. In the following, we interpret the unsteady pressure field in terms of the visualized interactions in the tip domain.

5. Wavelike nature of leading-edge region

On the basis of the flow visualization in figures 3 and 4, it is evident that the primary–secondary vortex pairs are associated with a convective wave motion along the surface of the edge which, in turn, should give rise to corresponding pressure waves along the surface. The central features of the incident unstable jet, the primary and secondary vortices, and a wavelike representation of them are given in figures 5(*a*, *b*). In figure 5(*b*), we show only the wavelike motion due to the pressure field along the surface of the edge, and that asociated with the unstable jet incident upon it. In linking 5(*a*) to 5(*b*), we have assumed for the moment that the primary and secondary vortices move at the same phase speed. The relation between the unstable flow patterns adjacent to the surface of the edge (figure 5*a*) and the pressure along

its surface (figure 5*b*) is a complex one, especially near the tip where flow separation sets in. Consequently, we expect a 'tip distortion region' to exist. Over this domain, the pressure field may well be a non-propagating one, in that the phase distribution of the pressure may simply reflect the rapid adjustment of the flow from a free jet to an unsteady boundary layer. Downstream of this region, however, where the primary and secondary vortices are well established, have the same frequency and travel with nearly the same phase speeds, the pressure field may be well represented by a simple wavelike propagation along the surface of the edge. In the following, we quantify these features.

6. Instantaneous pressure fields

The amplitude and phase distributions of the fluctuating pressure field along the edge follow from the cross-spectral analysis technique described in §2. Figure 6(*a*) shows these distributions for the low- and high-amplitude cases visualized in figure 3(*a*). The normalizing pressure amplitude $\tilde{p}_{\max}$ is the maximum amplitude along the surface for the respective cases under consideration; its value is larger for the high-amplitude case (right column) by a factor of 1.3. For both cases, we see that the shape of the pressure-amplitude distribution is very similar.

In essence, it is possible to consider this distribution as made up of two regions bounded by the pressure maximum: a region upstream of the amplitude maximum, which we call the 'near-tip' region, where the amplitude rapidly drops to a minimum as the tip is approached; and a region downstream of the amplitude maximum where the amplitude decreases as $(x'/\lambda)^{-a}$, with a value of $a = \frac{1}{2}$ describing the initial decrease.

The extent of the near-tip region is of the order 0.1λ, which is much smaller than the length of the edge. A necessary condition for interpretation of a Kutta condition in the leading-edge region is that the pressure must go to zero over a distance of the order of the length of the edge (D. G. Crighton 1984, private communication). Clearly, the rapid pressure decrease in the near-tip region suggests that imposition of a Kutta condition is inappropriate in simulations of the leading-edge region. We emphasize that this observation holds for the practical conditions of self-sustaining jet–edge oscillations where the characteristic velocity fluctuations of the approach shear layer can be of the order of 10 % of the centreline velocity (figure 2*b*). These conditions are inherent in the self-sustaining character of the oscillation and give rise to flow separation just downstream of the tip. It could well be that, in other situations where the characteristic amplitudes and frequencies are substantially lower, the onset of flow separation could be retarded or even precluded and the pressure would go to zero over a considerably larger streamwise distance. These features of the leading-edge region should be assessed in conjunction with what we know of the unsteadiness at a trailing-edge (Crighton 1985).

The region of pressure amplitude decrease as $(x'/\lambda)^{-a}$ commences at the pressure maximum, near the onset of flow separation. This is suggested by comparing the occurrence of the peak amplitude in figure 6(*a*) with the detailed timeline photos of figure 4. Comparison of these figures also suggests that the pressure amplitude induced by passage of the developed primary–secondary vortex pair is significantly less than that associated with the upstream flow separation leading to secondary-vortex formation; in the following we quantify these features.

Regarding the phase variations of the pressure fluctuations, distributions were obtained for two locations of the phase reference, one on the upper and the other on

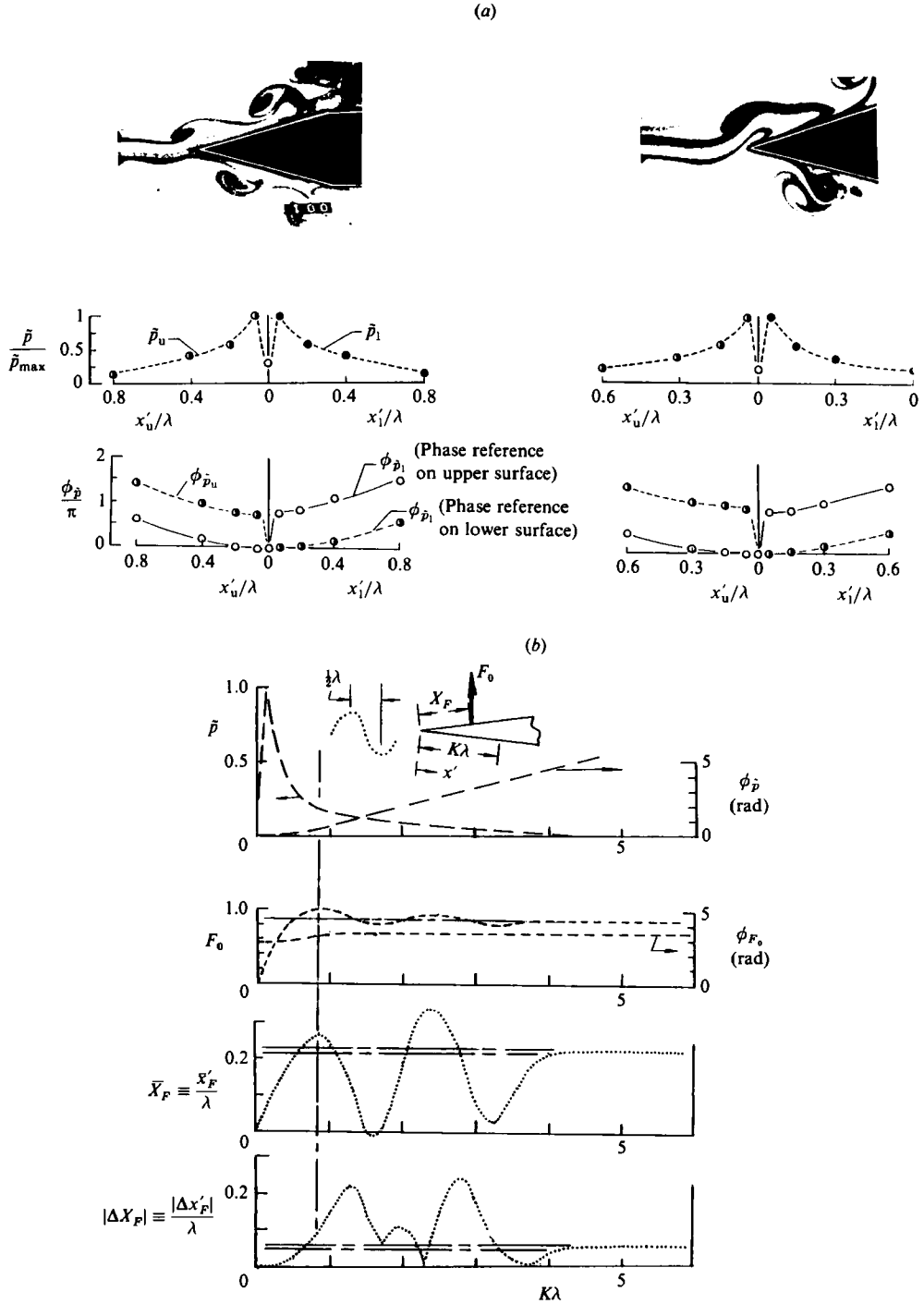

FIGURE 6. (*a*) Distributions of fluctuating pressure amplitude and phase along the upper and lower surfaces of the edge for low ($L/w = 3.25$) and high ($L/w = 4.5$) amplitudes of incident jet ($Re = 600$). (*b*) Force magnitude F_0 and phase ϕ_{F_0}, and its time-mean $\bar{X}_F$ and fluctuating $|\Delta X_F|$ location, all determined from the pressure amplitude $\tilde{p}$ and phase $\phi_{\tilde{p}}$. These parameters are plotted against $K\lambda$, which is the streamwise extent of the domain of integration of instantaneous pressure extending from the tip of the edge onwards.

the lower surface of the edge. There is a phase jump from 0 to $\approx\pi$ across the tip, in accord with the flow visualization of figure 3. Over the region $\phi \leqslant x'/\lambda \lesssim 0.20$, there is very little change in phase due to rapid flow distortion there. In this 'tip distortion region' the simplified wave propagation model of figure 5(*b*) is meaningless. Further downstream, however, these phase variations have a continuously increasing slope indicating a finite and decreasing wavelength $\lambda = 1/(\mathrm{d}\phi/\mathrm{d}x')$ due to the downstream-travelling vortex pattern. Details of the streamwise phase variations (and phase speeds) of the primary and secondary vortices in relation to those of the pressure field are discussed by Kaykayoglu (1984). In essence, as the primary vortex negotiates the tip of the edge, the phase speed increases then decreases, while the effective phase speed of the pressure field rapidly decreases downstream of the tip.

An important consequence of the pressure field at the tip of the edge is the location of the resultant force, which varies with time. If we consider the local pressure fluctuation at a given value of $x'/\lambda \equiv X$ to be of the form $\tilde{p}(X)\cos(\omega t+\phi(X))$, it is possible to determine the instantaneous pressure distribution. The instantaneous force $F_0\cos(\omega t+\theta)$ then follows from integration; its location $X_F(t)$ is defined as the sum of time-mean and fluctuating components, $X_F(t) \equiv \overline{X}_F + \Delta X_F(t)$. Figure 6(*b*) shows the pressure amplitude and phase distributions of figure 6(*a*), the resultant amplitude F_0 and phase ϕ_{F_0} of the force, and the time mean $\overline{X}_F$ and fluctuation $|\Delta X_F|$ amplitude of the force location; all of these parameters are plotted against $K\lambda$, the streamwise extent of the domain of pressure integration extending from $x' = 0$ at the tip of the edge to $x' = K\lambda$ downstream of it. We note that the actual data of figure 6(*a*) extend only to $K\lambda = 0.8$. Visualization shows that in these flows, the coherent vortex motion loses its highly organized character about one or two wavelengths downstream of the tip; consequently, we expect the pronounced spectral peak to rapidly attenuate, giving way to a smaller-amplitude, broadband spectral distribution of pressure. Accordingly, the amplitude of $\tilde{p}$ will tend to zero. In figure 6(*b*), we have extrapolated the pressure to zero and maintained a constant vortex phase speed well downstream of this location, i.e. to $K\lambda \approx 4$, in order to emphasize some of the peculiar features of the force location $\overline{X}_F \equiv \overline{x}'_F/\lambda$. As illustrated in figure 6(*b*), the force magnitude F_0, phase ϕ_{F_0}, and location $\overline{X}_F$ rapidly attain their near-asymptotic values within about one wavelength, i.e. $K\lambda \approx 1$. Particularly interesting, however, are the drastic variations in mean $\overline{X}_F$ and fluctuation $|\Delta X_F|$ locations of the force in the range $1 \leqslant K\lambda \leqslant 4$; they are due to the large moments of small instantaneous pressure at distances well downstream of the tip, which take on alternating sign due to the wavelike nature of the pressure field. It is evident that the asymptotic value of the fluctuation in force location $|\Delta X_F|$ is about 0.05λ, while that of the mean location $\overline{X}_F$ is about 0.22λ, which we approximate in subsequent discussions as a quarter wavelength. The fact that these asymptotic values are estimable from consideration of approximately the first wavelength only, $K\lambda \approx 1$, downstream of the tip is due in large part to the non-propagating nature of the pressure field in the near-tip region.

Most important for our considerations here is that $\overline{X}_F$ is a significant fraction of λ. This location of the force represents the effective (mean) centre of the source(s) of the upstream influence. In the seminal study of Powell (1961), the force is taken to be at the tip of the edge ($\overline{X}_F = 0$); its magnitude represents the strength of the dipole at the tip whose upstream influence closes the 'feed-back loop' of the self-sustained oscillation. Since the upstream influence to the nozzle exit is essentially instantaneous (at low speeds), the delay time in the oscillation cycle is due to the downstream-travelling jet instability of wavelength λ, over the distance L (neglecting $\overline{X}_F$) from the nozzle exit to the tip of the edge. Powell (1953) originally proposed the

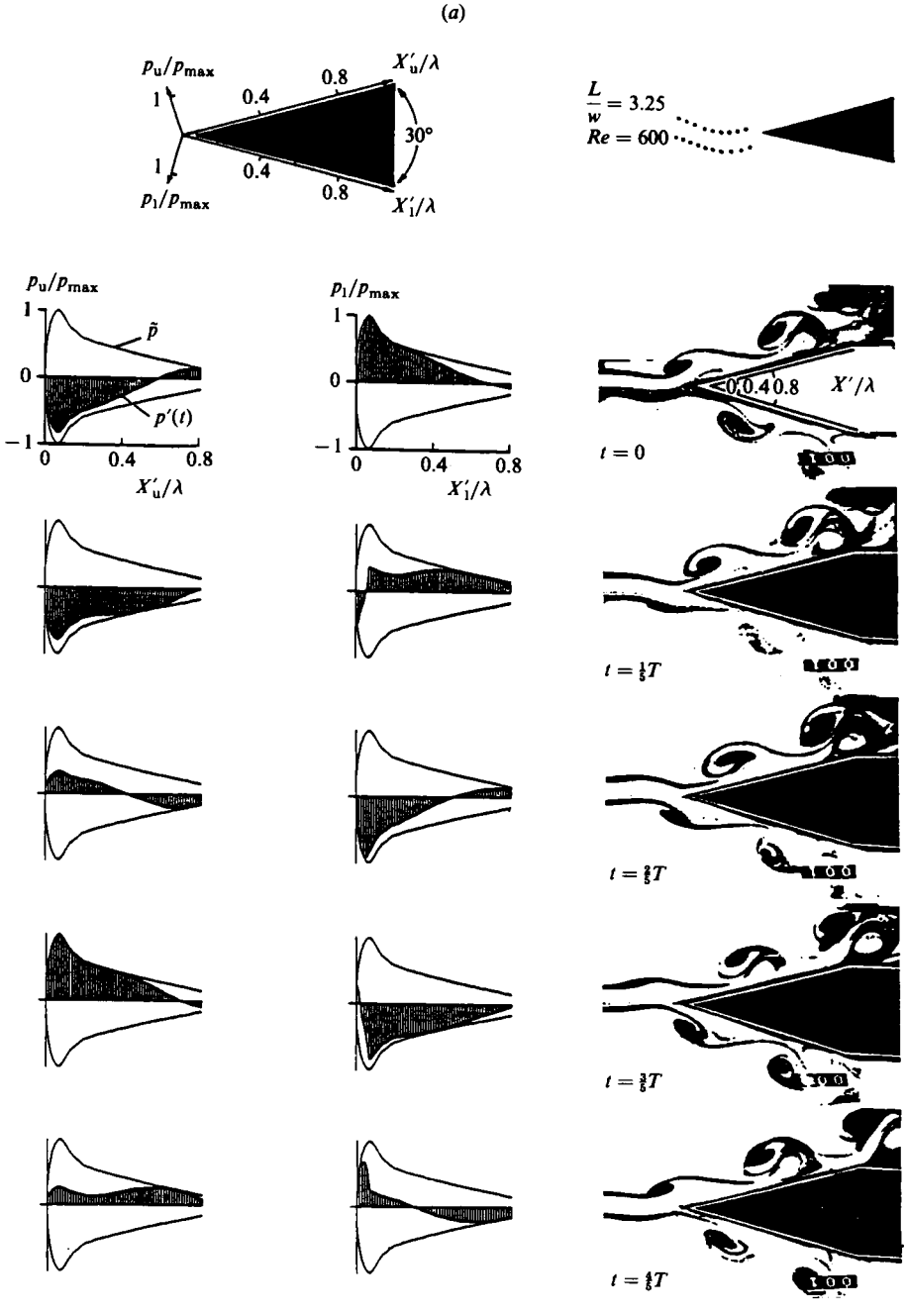

FIGURE 7. Instantaneous pressure fields on surface of leading edge, and corresponding visualized instabilities in leading-edge region for (*a*) low ($L/w = 3.25$) and (*b*) high ($L/w = 4.5$) amplitude oscillations of incident jet ($Re = 600$).

relation $L/\lambda = n + C$, where n is an integer, and $C = \frac{1}{4}$. The value of $C = \frac{1}{4}$ was based on the assumption that the generation of maximum pressure occurred as a vortex reached the edge; it corresponded to an averaged value, over a range of experimental conditions, of Brown's (1937) observations that the nonintegral part of L/λ had values predominantly between 0 and $\frac{1}{2}$. Clearly, the spirit of these original studies was

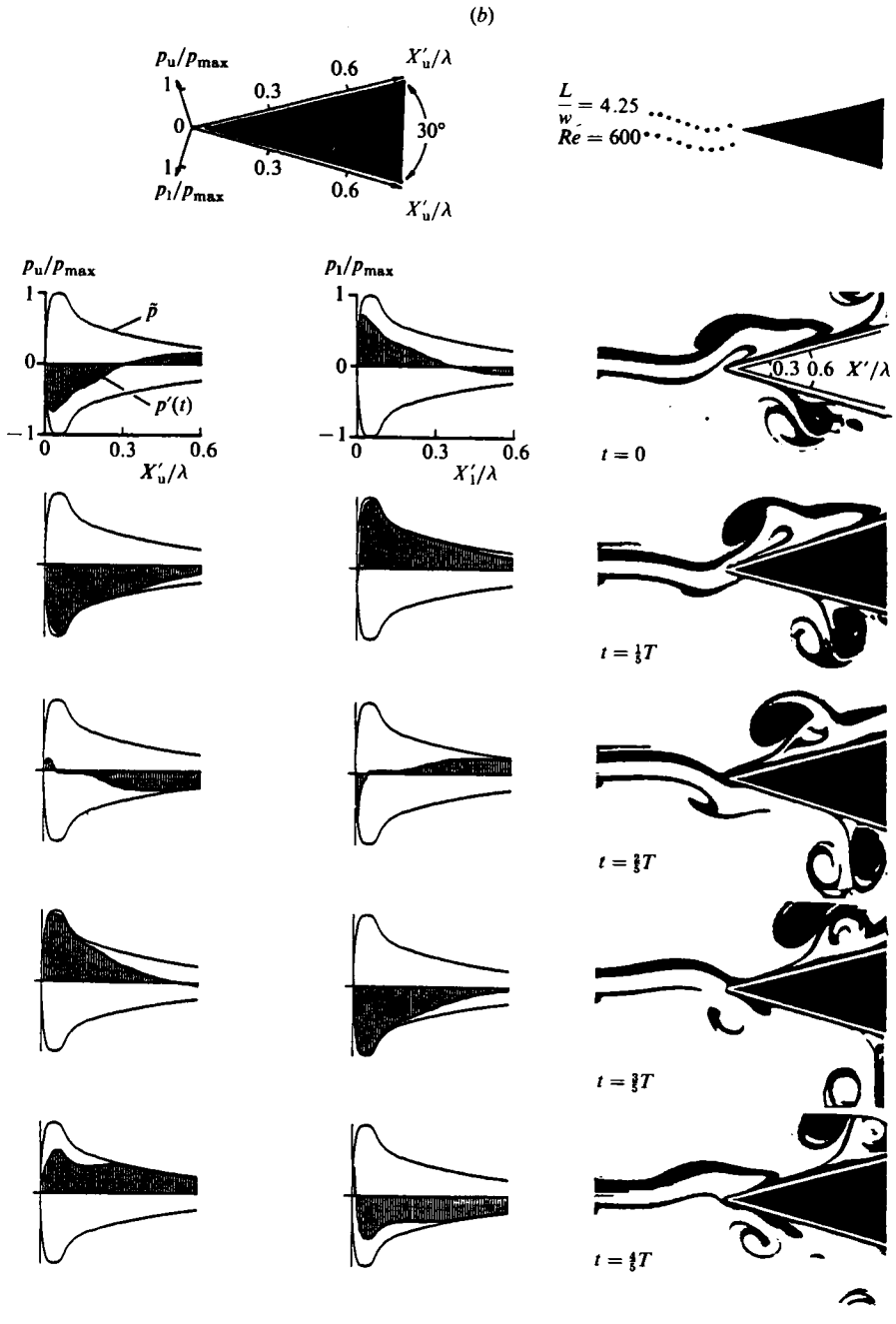

FIGURE 7(*b*). For caption see facing page.

to establish the physical framework for jet–edge oscillations; indeed, it has continued to provide valuable insight on which to base further studies. In a remarkable number of jet–edge investigations over the past two decades, as reviewed by Karamcheti *et al.* (1969), Rockwell & Naudascher (1979) and Rockwell (1983), attention has been focused on more-quantitative means of determining the constant C, accounting for the spatial non-homogeneity of the jet instability, by detailed measurements of

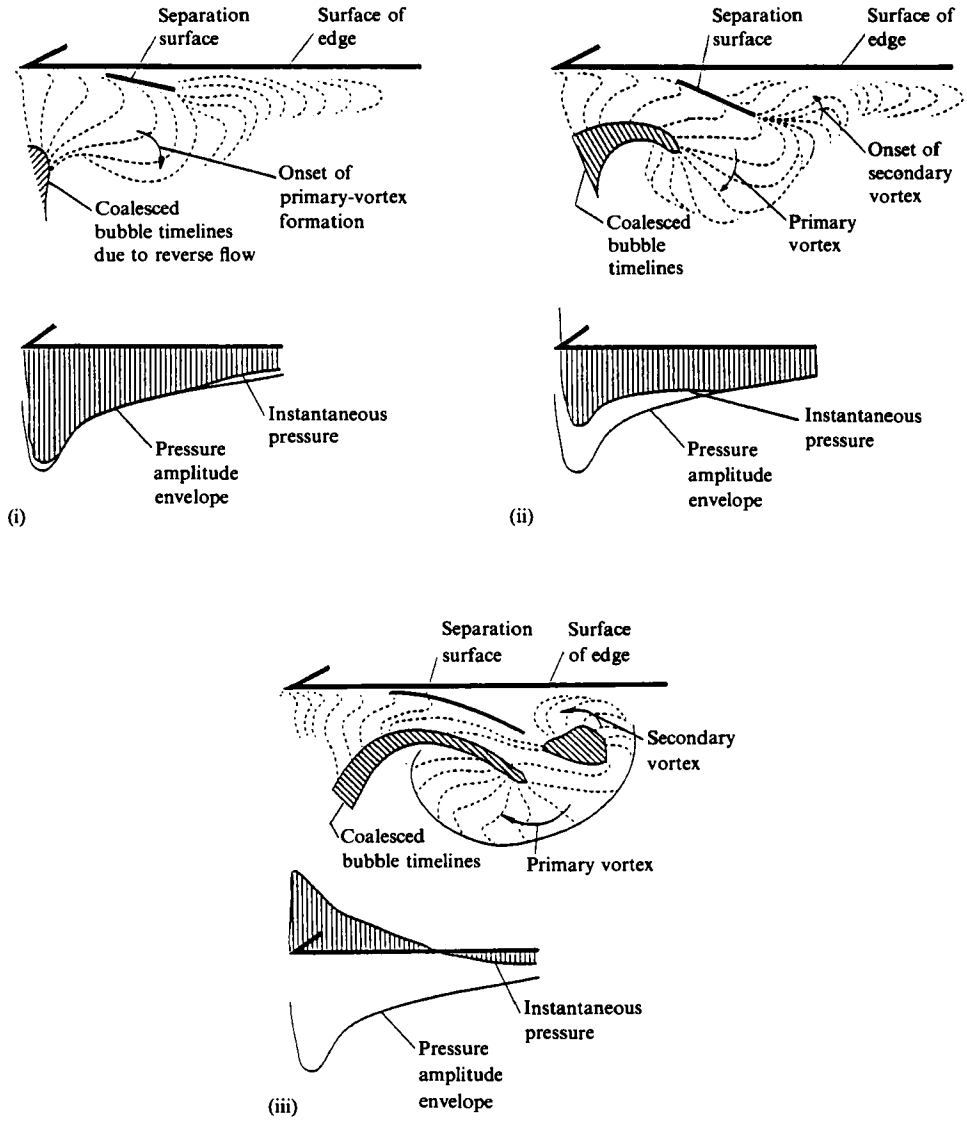

FIGURE 8. Correlation between digitized timeline distortion of figure 4 and instantaneous surface pressure for high-amplitude oscillation ($L/w = 4.5$; $Re = 600$).

streamwise phase variation over distance L. The conclusion to be drawn from these studies is that no universal value of C exists for self-sustained jet–edge oscillations. Remarkably, no consideration has been given to the possibility of a finite value of $\overline{X}_F$, which in effect increases the value of L. As demonstrated in the foregoing, $\overline{X}_F$ can be as high as $\frac{1}{4}\lambda$, which is the same order as $C\lambda$ found in a number of investigations in recent years. Moreover, streamwise phase measurements upstream of the edge (not discussed herein), indicate that $\overline{X}_F \sim \frac{1}{4}L$. Clearly, any refinement of the L/λ criterion proposed by Powell (1953) must include the $\overline{X}_F/\lambda$ contribution. Indeed, it was Powell (1953) who recognized early on the necessity of knowing details of the edge interaction region in determining the effective location of the sources. We

expect that subtle changes in the leading-edge interaction pattern will significantly alter the magnitude of $\bar{X}_F$, a matter which we discuss in §8.

The pressure-amplitude and phase distributions of figure 6 (*a*), along with correlation of the visualized edge interaction and the instantaneous pressure (see §2), allow construction of the instantaneous pressure fields at various instants of visualized edge interaction. Figures 7 (*a*, *b*) show the interactions for the two amplitude cases described in figure 3 (*a*). Maximum negative pressure occurs on the lower surface near the tip of the edge at t/T in the range $\frac{3}{5}$ to $\frac{4}{5}$. As already discussed in conjunction with figure 4, it corresponds to onset of roll-up of the primary vortex and flow separation from the surface near the tip of the edge. On the other hand, maximum positive pressure on the lower surface occurs between a well-formed primary vortex that has passed the tip of the edge and the oncoming instability wave that is about to roll-up into a primary vortex.

The correlation between the instantaneous pressure and a digitized representation of the timeline visualization of figure 4 is shown in figure 8 for three representative instants of flow development in the leading-edge region: (i) onset of primary-vortex formation and separation of flow leading to formation of a separation surface; (ii) onset of secondary-vortex formation; and (iii) further development of the primary–secondary vortex pair as it moves downstream. It is evident that the negative pressure amplitude associated with the onset of flow separation in the tip region (see (i)) is substantially larger than that due to passage of the primary–secondary vortex pair (see (iii)). From these observations, as well as those of figure 6 (*a*), we conclude that the x^{-a} behaviour of the pressure amplitude is mainly due to the large pressure gradient leading to onset of flow separation and only mildly influenced by the pressure induced by passage of the vortex pair downstream of separation.

7. Asymmetrical shear layer–edge interactions

In the foregoing, we have considered the case of a leading edge at the centreline of the jet; however, if the edge is not symmetrically disposed in the jet, one expects the propagating vortex patterns and pressure fields to differ on the upper and lower surfaces.

Figure 9 shows the high-amplitude oscillation at three values of dimensionless offset. At $\eta/b = 0$, already discussed in conjunction with figure 3 (*b*), there is rapid development of the counter-rotating vortex pair on the underside of the edge. At increasing values of offset, however, there is substantial delay in growth of the vortex pair; the rapid shooting of the pair away from the surface, evident for $\eta/b = 0$, is not as pronounced. Moreover, if one examines the wavelength between the primary vortex formed at the tip and the downstream counter-rotating vortex pair along the bottom surface of the edge (see the fourth row of figure 9), it is evident that the wavelength between them decreases at larger offset.

The photos of figure 9 suggest little alteration of the amplitude of transverse oscillations of the jet in its upstream region. This observation is quantified in figure 10; the left sketch indicates that the effect of increased offset is to decrease the amplitude of the secondary peaks at the sides of the jet, while the primary peak (on the side towards which the wedge is moved) tends to show an increase in amplitude. Most important for our considerations here is the fact that as the edge is displaced off centreline, it sees large changes in the amplitude of the $\tilde{u}$-fluctuation; this trend is indicated schematically in figure 10. Consequently, one expects the pressure at the tip of the edge to rise accordingly. Neglecting, for the moment, the effects of distortion

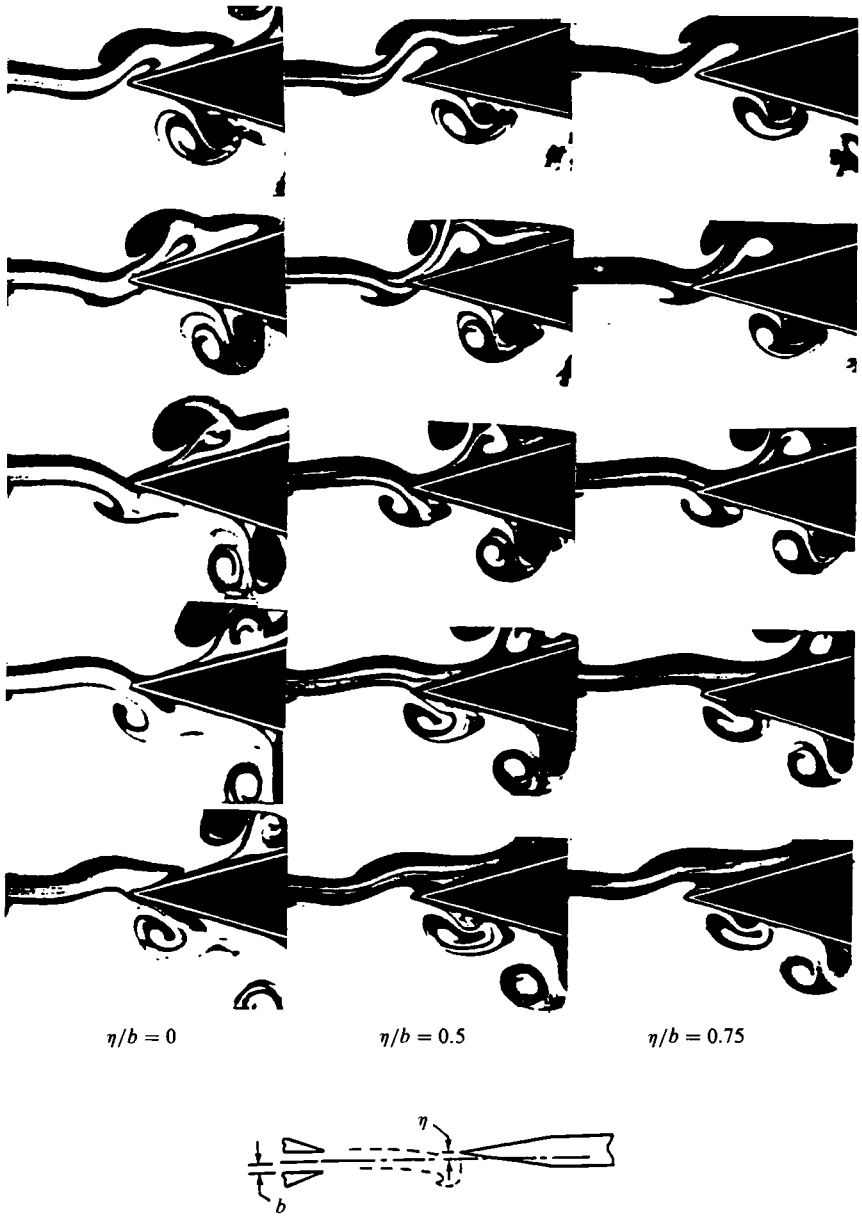

FIGURE 9. Effect of asymmetrical location of edge with respect to jet centreline on leading-edge instabilities, for case of high-amplitude oscillating jet incident upon leading edge ($Re = 600$; $L/w = 4.5$).

as the tip is approached, and treating the flow as quasi-parallel ($\bar{v} \approx 0$), the amplitude of the fluctuating pressure may be linearized to $\tilde{p} \sim \rho \bar{u} \tilde{u}$. From the measurements of $\bar{u}(y)$ described by Kaykayoglu (1985) and the values of $\tilde{u}$ of figure 10, the values of the product $\tilde{u}\bar{u}/U_{\mathbf{c}}^2$ at dimensionless offsets $\eta/b = 0$, 0.5, and 0.75 are 0.02, 0.064, and 0.068. Neglecting effects of distortion at the edge, we expect the leading-edge pressure to increase accordingly. In fact, the pressure distributions of figure 10 show

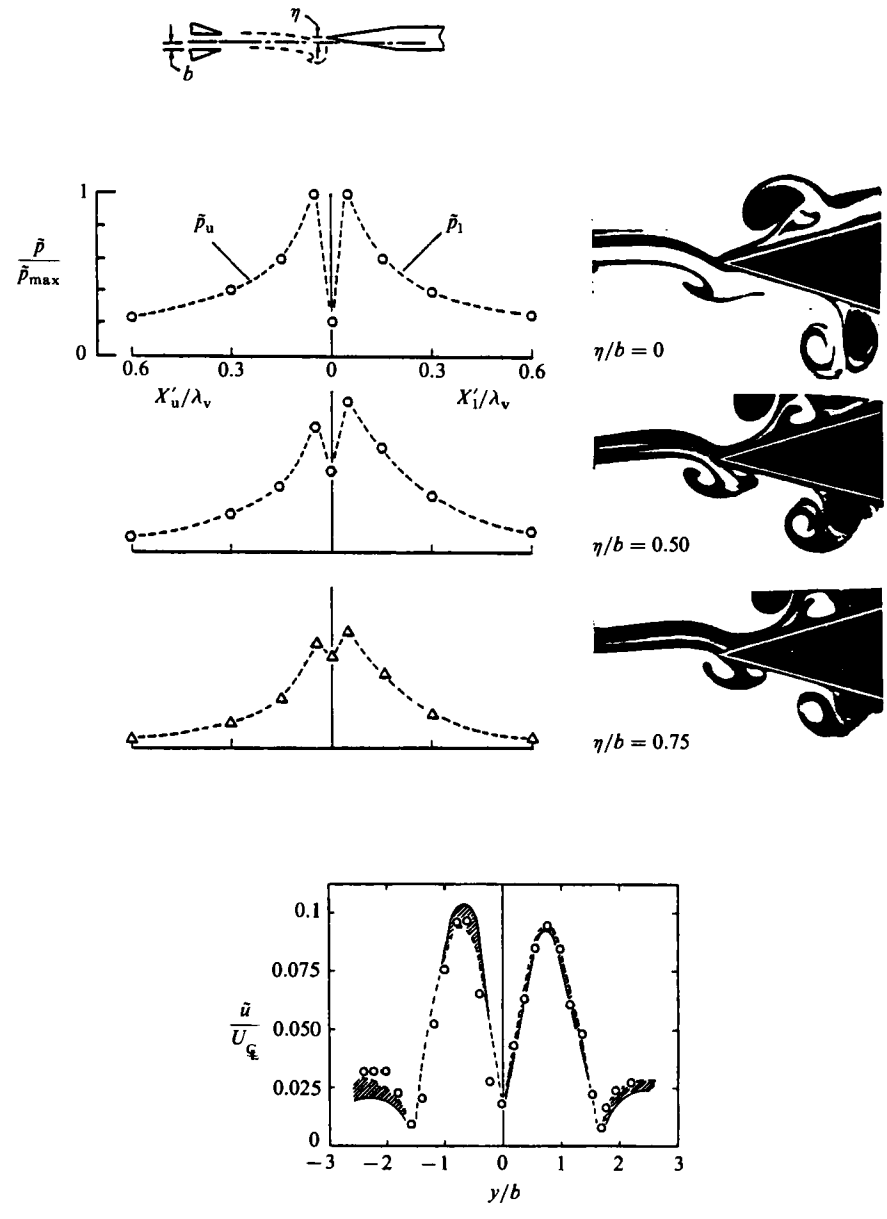

FIGURE 10. Effect of offset of leading-edge on amplitude distribution of fluctuation velocity and corresponding pressure amplitudes in leading-edge region, for the higher-amplitude fluctuating jet incident upon the edge ($Re = 600$; $L/w = 4.5$).

that the tip pressure amplitude increases substantially with increasing offset. This offset gives, in turn, a decrease in maximum pressure amplitude immediately downstream of the tip due to the alteration in interaction mechanism. That is, there is slower, and less pronounced, development of the vortex pair along the lower surface and delayed vortex development along the upper surface as the offset η increases.

8. Concluding remarks

In the foregoing, we have addressed loading of the leading edge in conjunction with the unsteady flow structure there; experimental conditions corresponded to those of the classical, single-frequency jet–edge oscillation at low speed. The form of the unsteady pressure amplitude is characterized by two regions, one near the tip, and the other downstream of it; these regions are bounded by the maximum pressure amplitude. In the near-tip region the pressure drops to a minimum over a relatively short streamwise distance which, in turn, is determined by the distance downstream of the tip at which there is onset of separation. The second region, immediately downstream of the near-tip domain is characterized by an x^{-a} decrease in pressure amplitude, where $a = \frac{1}{2}$ for the initial decrease. The drop in pressure as the tip of the edge is approached is because flow separation occurs downstream of, rather than at, the tip of the edge. The fact that separation should not occur from the tip itself is deducible from considering the fluctuating angle of attack of the approach shear layer. This angle-of-attack distribution, which follows from consideration of the fluctuation-velocity amplitudes and phases in conjunction with the mean flow, shows a minimum along the centreline of the jet. When the tip amplitude is increased, arising from displacement of the edge off centreline, the x^{-a} behaviour of the pressure amplitude upstream of the tip region still persists. This persistence is because flow separation downstream of the tip always occurs for the range of initial tip fluctuation levels examined herein; it is this onset of separation that gives rise to the peak pressure amplitude, allowing x^{-a} behaviour irrespective of the initial level at the tip.

Since the streamwise extent of the near-tip region is small, it seems most appropriate to simulate the pressure field as singular according to x^{-a}. We note, however, that drop in pressure as the tip is approached could occur over longer streamwise distances when the fluctuation level of the approach shear layer decreases. This could best be accomplished by perturbing a laminar approach shear layer, free from the upstream-influence effects of the classical jet–edge configuration. Although such an experimental undertaking is difficult to establish practically, in principle it seems that if the onset of flow separation could be retarded or precluded, then the streamwise extent of the near-tip region could be substantially extended, opening up the possibility for a leading-edge Kutta condition.

The flow structure in the leading-edge region involves the growth of a primary vortex there, emanating from the instability of the jet shear layer, and formation of a secondary vortex from separation of the viscous layer on the surface of the edge. It is shown that the peak pressure amplitude is associated with the onset of flow separation; in comparison, the pressure amplitude induced by passage of the primary–secondary vortex pair in the downstream region of the edge is overshadowed by that induced by separation. Therefore, we attribute the x^{-a} variation of pressure as mainly due to the onset of flow separation, being only mildly influenced by vortex dynamics in the region immediately downstream of it.

We found the integrated loading, i.e. resultant force, acting on the leading-edge region, to be at a distance of about $\frac{1}{4}\lambda$ downstream of the tip. If we view the location of this force as the centre of the effective source, or distribution of sources, that gives rise to the upstream influence, then it is clear that assuming the force to be at the tip itself is not a reasonable approximation. In essence, this means that the geometric length from the nozzle exit to the tip of the edge is not the appropriate lengthscale for formulating a 'phase-locking' criterion for self-sustaining oscillations. Research efforts over the past two decades on this class of flows (see reviews of Karamcheti

et al. 1969; Rockwell 1983) have focused on finding a universal phase criterion based on the streamwise-phase-variation nozzle exit and the tip of the edge; no such criterion has emerged. On the basis of our findings, such attempts are meaningful only if considered in conjunction with the effective centre of the source(s) downstream of the tip, which will be a function of the leading-edge interaction mechanism. For certain types of leading-edge interactions, such as those of a concentrated vortex impinging directly on the tip (Kaykayoglu & Rockwell 1986), whereby separation occurs from the tip itself owing to a fundamentally different mechanism than described herein, the pressure has maximum amplitude at the tip, and decays over a substantially shorter streamwise distance than for the type of interaction described in the foregoing. Correspondingly, the effective centre of the force, and thereby the source(s), are very near the tip.

The phase shift between the force on the edge and the jet motion is primarily determined by the near-tip region of the edge, owing to the negligible streamwise phase variations of pressure and correspondingly high pressure amplitude in that region. In fact the phase variation of the fluctuating pressure exhibits negligible phase change over distances as long as one-fifth of a wavelength from the tip of the edge. The fact that the surface pressure field is non-propagating in this near-tip region is particularly interesting in view of the fact that the formation and convection of the primary vortex in the outer region of the flow represents a propagating wave; it is clearly a continuation of the propagating instability wave from the upstream flow. It is the severe flow distortion associated with onset of separation in the near-tip region that produces the non-propagating pressure there which, in turn, gives rise to highly correlated loading and allows the tip region to dictate the phasing of the loading over the surface of the edge.

In the foregoing, we have emphasized the importance of the fundamental mechanism of secondary-vortex formation, which occurs in conjunction with the formation of the primary vortex, aided by the distortion in the near-tip region. Of course, even in the case of a wall of infinite extent, the presence of a primary vortex of sufficient circulation will induce a secondary vortex. The experiments of Harvey & Perry (1971) and Horne & Karamcheti (1979) clearly illustrate this phenomenon for a trailing vortex–ground interaction and a planar (shear layer) vortex–wall interaction respectively. An analogous type of secondary-vortex formation for the case of axisymmetric 'loop' vortices impinging orthogonally upon a flat plate has been studied by Magarvey & McLatchy (1964), C.-M. Ho (1979, private communication), Schneider (1980), Cerra & Smith (1983), Ho (1983), and Didden & Ho (1985). These studies address the secondary vortex produced by the primary loop vortex–wall interaction. In this class of flows, the pressure gradients associated with the mean-flow distortion are substantial. The results of pressure measurements of Didden & Ho (1985) are similar to ours: the onset of flow separation produces the highest pressure-fluctuation amplitude. We emphasize, for the case examined herein, that the mean boundary layer along the surface of the leading edge is very thin; yet wall viscous effects are central in producing the secondary vortex. Once the flow separates, however, it may be possible to describe the growth of the secondary vortex using inviscid stability concepts applied to an inflexionally shaped shear layer, much in the spirit of an unstable mixing layer. Indeed, Didden & Ho (1985) suggest that viscous effects may not be important. This interpretation is also encouraged by observations of Homa & Rockwell (1983) for a vortex pair past a very small cylinder; the secondary vortex experiences rapid amplification downstream of the cylinder.

With regard to the general concept of onset of flow separation due to the passage

of a primary vortex, Walker (1978) describes theoretically such an interaction with a primary line vortex passing above a flat plate for the case of a boundary-layer profile; his calculations show rapid thickening of the boundary layer and formation of a secondary recirculation zone. Subsequent investigations by Doligalski, Smith & Walker (1980) and Doligalski & Walker (1984) address the consequence of further aspects such as sign and speed of the primary line vortex. Analogies with the present work must be approached with caution, however, in view of basic differences in mean-flow profiles and concentrations of vorticity.

Primary support for this work was provided by the Office of Naval Research, with supplemental support by the National Science Foundation. The Volkswagen Foundation contributed to development of certain of the flow-visualization techniques employed herein. The authors are grateful to Dr Thomas Staubli for computing the force parameters of figure 6, and to him and Professor M. V. Morkovin for insightful criticisms of the manuscript.

REFERENCES

Brown, G. B. 1937 Vortex motion causing edge tones. *Proc. Phys. Soc.* **49**, 493–507.

Cerra, A. & Smith, C. 1983 Experimental observations of vortex ring interaction with the fluid adjacent to a surface. *Rep.* SM-4, Lehigh University, AFOSR TR-84-0130, ADA 138999.

Crighton, D. G. 1981 Acoustics as a branch of fluid mechanics. *J. Fluid Mech.* **106**, 261–298.

Crighton, D. G. 1985 The Kutta condition in unsteady flow. *Ann. Rev. Fluid Mech.* **17**, 411–445.

Didden, N. & Ho, C.-M. 1985 Unsteady separation in a boundary layer produced by an impinging jet. *J. Fluid Mech.* **160**, 235–256.

Doligalski, T. L., Smith, C. R. & Walker, J. D. A. 1980 A production mechanism for turbulent boundary-layers. In *Viscous Drag Reduction* (ed. G. Gettough); *Prog. Astro. Aero.* **72**, 47–72.

Doligalski, T. L. & Walker, J. D. A. 1984 The boundary layer induced by a convected two-dimensional vortex. *J. Fluid Mech.* **139**, 1–28.

Goldstein, M. E. 1978 Characteristics of the unsteady motion on transversely sheared mean flows. *J. Fluid Mech.* **84**, 305–329.

Goldstein, M. E. 1979 Scattering and distortion of the unsteady motion on transversely sheared mean flows. *J. Fluid Mech.* **91**, 601–632.

Goldstein, M. E. 1981 The coupling between flow instabilities and incident disturbances at a leading edge. *J. Fluid Mech.* **104**, 217–246.

Harvey, J. K. & Perry, F. J. 1971 Flow field produced by trailing vortices in the vicinity of the ground. *AIAA J.* **9**, 1659–1660.

Homa, J. & Rockwell, D. 1983 Vortex–body interaction. *Bull. Am. Phys. Soc.* **28**, 1365.

Horne, C. & Karamcheti, K. 1979 Experimental observations of a two-dimensional planar wall jet. *AIAA Paper* 79-0208.

Howe, M. S. 1981 The role of displacement thickness fluctuations in hydroacoustics, and the jet-drive mechanism in the flue organ-pipe. *Proc. R. Soc. Lond.* A **374**, 543–568.

Karamcheti, K., Bauer, A. B., Shields, W. L., Stegen, G. R. & Wooley, J. P. 1969 Some features of an edge-tone flow field. In *Basic Aerodynamic Noise Research, NASA SP* 207; *conference held at NASA Headquarters, Washington, D.C., July* 14–15, pp. 275–304.

Kaykayoglu, R. 1984 Interactions of unstable shear layers with leading edges and associated pressure fields. Ph.D. dissertation, Department of Mechanical Engineering and Mechanics, Lehigh University.

Kaykayoglu, R. & Rockwell, D. 1985 Vortices incident upon a leading edge: instantaneous pressure fields. *J. Fluid Mech.* **156**, 439–461.

Kaykayoglu, R. & Rockwell, D. 1986 Unstable jet-edge interaction. Part 2: Multiple frequency pressure fields. *J. Fluid Mech.* **169**, 151–172.

LUCAS, M. & ROCKWELL, D. 1984 Self-excited jet: upstream modulation and multiple frequencies. *J. Fluid Mech.* **147**, 333–352.

MAGARVEY, R. H. & MCLATCHY, C. S. 1964 The disintegration of vortex rings. *Can. J. Phys.* **42**, 684–689.

POWELL, A. 1953 On edge tones and associated phenomena. *Acustica* **3**, 233–242.

POWELL, A. 1961 On the edgetone. *J. Acoust. Soc. Am.* **33**, 395.

ROCKWELL, D. 1983 Oscillations of impinging shear layers. *AIAA J.* **21**, 645–664.

ROCKWELL, D. & NAUDASCHER, E. 1979 Self-sustaining oscillations of impinging free shear layers. *Ann. Rev. Fluid Mech.* **11**, 67–94.

SCHNEIDER, P. E. M. 1978 Morphologisch-phänomenologische Untersuchung der Umbildung von Ringwirbeln, die Körper anströmen. *Max-Planck-Institut für Strömungsforschung Bericht Nr.* 14/1978, Göttingen.

WALKER, J. D. A. 1978 The boundary layer due to rectilinear vortex. *Proc. R. Soc. Lond.* A **359**, 167–188.